Lawrence Berkeley National Laboratory

Title

Accurate X-Ray Spectral Predictions: An Advanced Self-Consistent-Field Approach Inspired by Many-Body Perturbation Theory

Permalink

https://escholarship.org/uc/item/3296b3mk

Authors

Liang, Yufeng
Vinson, John
Pemmaraju, Sri
et al.

Accurate X-Ray Spectral Predictions: An Advanced Self-Consistent-Field Approach Inspired by Many-Body Perturbation Theory

Yufeng Liang,[1] John Vinson,[2] Sri Pemmaraju,[1] Walter Drisdell,[3] Eric L. Shirley,[2] and David Prendergast[1]

[1] *The Molecular Foundry, Lawrence Berkeley National Laboratory, Berkeley, CA 94720, USA*
[2] *National Institute of Standards and Technology (NIST), Gaithersburg, MD 20899, USA*
[3] *Chemical Sciences Division, Lawrence Berkeley National Laboratory, Berkeley, CA 94720, USA*

Constrained-occupancy delta-self-consistent-field (ΔSCF) methods and many-body perturbation theories (MBPT) are two strategies for obtaining electronic excitations from first-principles. Using the two distinct approaches, we study the O $1s$ core excitations that have become increasingly important for characterizing transition-metal oxides and understanding strong electronic correlation. The ΔSCF approach, in its current single-particle form, systematically underestimates the pre-edge intensity for chosen oxides, despite its success in weakly correlated systems. By contrast, the Bethe-Salpeter equation within MBPT predicts much better lineshapes. This motivates one to reexamine the many-electron dynamics of X-ray excitations. We find that the single-particle ΔSCF approach can be rectified by explicitly calculating many-electron transition amplitudes, producing X-ray spectra in excellent agreement with experiments. This study paves the way to accurately predict X-ray near-edge spectral fingerprints for physics and materials science beyond the Bethe-Salpether equation.

X-ray absorption spectroscopy (XAS) is a powerful characterization technique in physics, chemistry, and materials science, owing to its element specificity and orbital selectivity. With the help of density-functional theory (DFT), the interpretation of XAS is greatly facilitated by simulating spectral fingerprints for hypothetical structures from first-principles. Satisfactory X-ray absorption spectra have been simulated across a wide range of systems from small molecules [1, 2] to condensed matter [3–9] and even complex interfaces [10].

In this letter, we introduce a novel first-principles theory for simulating X-ray absorption spectra extending the constrained-occupancy delta-self-consistent-field (ΔSCF) method [6, 7, 9]. The ΔSCF method assumes a fixed core-hole potential and employs only single-particle orbitals for finding transition amplitudes. It is generally thought this theory cannot capture certain many-electron effects as incorporated in many-body perturbation theories, such as the Bethe-Salpeter Equation (BSE) [11–14]. However, if the one-body transition amplitude in the ΔSCF method is recast into a many-body formalism, we show that the method can in fact capture many-electron effects in X-ray excitations. Furthermore, we outline how the excitation spectrum can be enriched by considering multiple electron-hole (e-h) excitations, permitting extensions beyond the BSE, on the level of the Mahan-Noziéres-De Dominicis (MND) theory[15, 16].

For our examples, we choose the O K edges ($1s \rightarrow np$ transitions) of transition-metal oxides (TMOs) to illustrate the utility of the many-body ΔSCF method. The study of the O K edges for TMOs is fueled by the quest for next-generation energy materials, for rechargeable battery cathodes [17–20], fuel cells [21, 22], water-splitting catalysts [23–25], and transparent conductive layers [26]. Many of these materials are TMOs with complex chemical properties due to their d orbitals. Addi-

tionally, XAS has been employed to understand electron correlations inherent in TMOs, such as metal-insulator transitions [27–29], high-T_c superconductivity [30, 31], and emergent phenomena at perovskite interfaces [32]. XAS can also serve as powerful guides to advance theories for correlated electron systems, including the DFT+U method [33], dynamical mean-field theory [34], and exact diagonalization approaches [35, 36]. In almost all of the aforementioned examples [17, 19–21, 23–28, 30–33, 35, 36], there are measurements at the O K edge. Despite its utility, very few studies have simulated this absorption edge for TMOs from first-principles.

Five TMOs are selected for benchmarking: the rutile TiO_2, VO_2, and CrO_2 as well as the corundum α-Fe_2O_3 and the perovskite $SrTiO_3$. They vary greatly in structure, band gap, or magnetism. The rutile VO_2 ($> 340K$) and CrO_2 are metallic, whereas TiO_2 and $SrTiO_3$ are insulating. CrO_2 is ferromagnetic (FM) while Fe_2O_3 is antiferromagnetic (AFM). The O K edges from previous experiments [23, 27, 37–39] are shown in Fig. 1 (a). These spectra are angularly averaged except for CrO_2, where the polarization is perpendicular to the magnetization axis [38]. The TM-3d-O-2p hybridization manifests as sharp double peaks around 530 eV, which result from the t_{2g}-e_g splitting in the octahedral field. The intensity ratio of the two peaks often serves as a diagnostic tool. Understanding gained through these simple TM compounds will find great utility in interpreting XAS for more complex contexts, e.g., liquids, interfaces, heterogenous materials, where other characterization techniques such as X-ray diffraction are less effective. For instance, the O K-edge peak intensities have been used to deduce oxygen redox chemistry in rechargeable battery cathodes [20], and yet the correlation between experimental spectra and first-principles modeling of structures remains to be established, in the absence of accurate predictions of
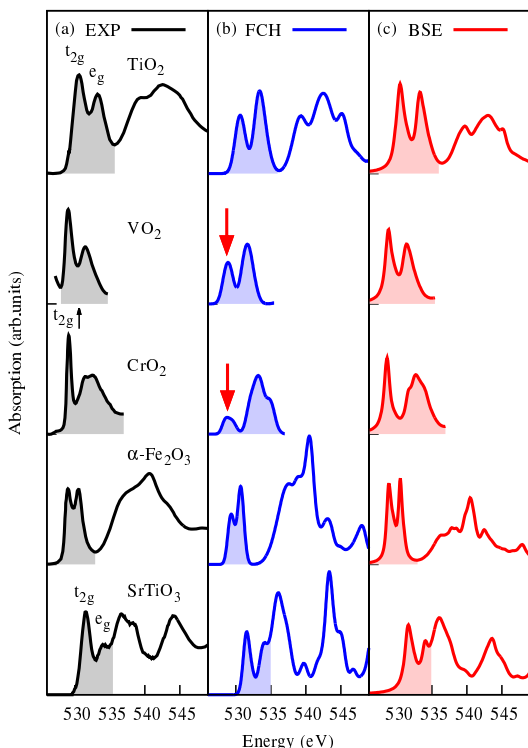
FIG. 1. A comparison of experimental O K edges (a) with the simulated spectra by the FCH approach (b) and BSE (c). The pre-edge regions are covered by shaded areas. Spectra are normalized according to the e_g peak intensity. The severely underestimated t_{2g} peaks are marked by red arrows.

the near-edge lineshape.

The X-ray absorbance $\sigma(\omega)$ is obtained from Fermi's golden rule

$$\sigma(\omega) \propto \omega \sum_f |\langle \Psi_f | \boldsymbol{\epsilon} \cdot \boldsymbol{R} | \Psi_i \rangle|^2 \delta(E_f - E_i - \hbar\omega) \quad (1)$$

where $\boldsymbol{\epsilon}$ and $\boldsymbol{R}$ are the photon polarization and many-body position operator respectively. $|\Psi_i\rangle$ is the initial (ground) state and $|\Psi_f\rangle$ is any excited eigenstate of the system, while E_i and E_f are their energies. Predicting X-ray absorption requires: (a) an accurate prediction of the excitation energies E_f and (b) a reliable approximation to the amplitude $\langle \Psi_f | \boldsymbol{\epsilon} \cdot \boldsymbol{R} | \Psi_i \rangle$. We first contrast the single-particle ΔSCF core-hole approach and the BSE using the five TMOs, and identify a systematic failure in the current ΔSCF method. We argue that the failure is due to the omission of many-electron response to the core hole, which motivates us to develop an advanced ΔSCF approach by using many-electron wavefunctions instead of single-particle orbitals.

ΔSCF and BSE Approaches In the ΔSCF core-hole approach the core-excited atom is treated as a single impurity with one electron removed from the excited core level. Depending on whether or not the X-ray photoelectron is included, it is termed as an excited-electron

and core-hole (XCH) or full core-hole (FCH) calculation [6, 7, 9]. One places the core-excited atom in a sufficiently large supercell and then finds the equilibrated electron density using constrained-occupancy DFT. This equilibrated state, with the presence of a core hole, is referred to as the *final state*[13], and that of the pristine system as the *initial state*. The working approximation is to use single Kohn-Sham orbitals for finding the transition amplitude

$$\langle \Psi_f | \boldsymbol{\epsilon} \cdot \boldsymbol{R} | \Psi_i \rangle \approx S \langle \tilde{\psi}_f | \boldsymbol{\epsilon} \cdot \boldsymbol{r} | \psi_h \rangle \quad (2)$$

where $\tilde{\psi}_f$'s are the unoccupied orbitals in the final state (with tilde) and ψ_h is the core orbital in the initial state. S is a many-body overlap that reflects the excited-state response of the remaining electrons other than the photoexcited one, and is normally treated as a constant in the sudden approximation [40]. The excitation spectrum $E_f - E_i$ is approximated based on differences in DFT orbital energies, $\tilde{\varepsilon}_f - \varepsilon_h$, with some further realignment reflecting the local atomic context and the experimental energy scale [41].

To account for strong electron correlations in TMOs, the DFT+U theory [33] is employed where the DFT energy is captured by the Perdew-Burke-Ernzerhof (PBE) functional, and the on-site Coulomb potential U are from Ref. [42]. We interpret the DFT+U orbital energies as quasiparticle (QP) energies and perform FCH rather than XCH calculations so as not to favor any particular occupation. More numerical details can be found in the Supplemental Material [56].

Strikingly, the FCH approach systematically underestimates the intensity of the near-edge peak associated with the t_{2g} manifold for all selected TMOs (Fig. 1 (b)) . The t_{2g} peak at ~ 529.2eV of CrO_2 [38] suffers from the most severe underestimation. It becomes a weak, broad feature in the FCH simulation as compared to the strong, sharp peak in experiment. The t_{2g}-e_g peak intensity ratios of VO_2 and Fe_2O_3 are also too low - both are predicted as 0.7, compared with 1.7 and 1.0 as measured, respectively.

In the BSE formalism [12, 43, 44], the final state is assumed to be a superposition of effective e-h pairs and the matrix elements are calculated as

$$\langle \Psi_f | \boldsymbol{\epsilon} \cdot \boldsymbol{R} | \Psi_i \rangle = \sum_c A_c^{f*} \langle \psi_c | \boldsymbol{\epsilon} \cdot \boldsymbol{r} | \psi_h \rangle \quad (3)$$

where ψ_c's are the *initial-state* orbitals and c iterates over *empty* orbitals only. The exciton amplitude A_c^f and energy E_f can be solved from the BSE as in Ref. [11–14]. The core-level BSE calculations in this work employ the OCEAN code [14, 45].

As is shown in Fig. 1 (c), the BSE substantially improves on the O K-edge line shapes. The "t_{2g}" peak intensity is retrieved for each investigated TMO, particularly for CrO_2. The simulated t_{2g}-e_g intensity ratios are
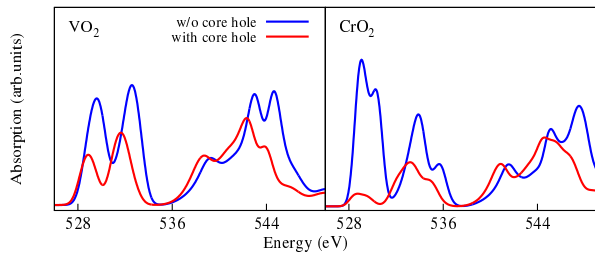
FIG. 2. (Color Online) A comparison of the spectra with and without (w/o) the core hole in the ΔSCF calculations.

almost as measured for TiO_2, α-Fe_2O_3, and $SrTiO_3$ (below 537 eV). These BSE spectra are also in better agreement with experiments than the previous results using the initial-state rule [46, 47].

In fact, the core-hole effects predicted by the ΔSCF method in these oxides are counterintuitive. Typically, excitonic effects tend to sharpen the absorption edge due to e-h attraction [5, 11, 12, 43]. In Fig. 2, we show the core-hole effects from ΔSCF by comparing the initial- and final-state spectra. The core-hole attraction does redshift the spectra by over 1 eV in both the TM $3d$ pre-edge and the $4sp$ [48] region (near 544 eV). However, the FCH core-hole effect substantially reduces the t_{2g} peak intensity. Similarly underestimated pre-peak intensity was encountered before [49–51] but no satisfactory explanation has been provided to date.

With this comparison, we can now explain why the one-body ΔSCF formalism tends to underestimate the peak intensity. The single-particle approximation in Eq. (2), $S\langle\tilde{\psi}_f|\boldsymbol{\epsilon}\cdot\boldsymbol{r}|\psi_h\rangle$, does not contain any information about the initial state of the valence electrons, when S is a constant. The spectrum is found by summing up single-particle transitions in the final state in which the valence electrons have already equilibrated with the core hole. The final-state picture alone does not reflect the full process of X-ray excitations: first a core hole is generated by an X-ray photon, then the valence electrons begin to relax in presence of the core-hole potential. This is why the final-state spectra predicted by the one-body formalism can be subject to spurious charge transfer effects, if the electron density happens to transfer onto the optically active orbitals due to core-hole attraction. In the above examples of O $1s$ excitations, a substantial amount of electron density is transferred into the $2p$ character local to the excited O (0.55 e^- for TiO_2 and 0.72 e^- for CrO_2), which blocks some bright transitions from $1s \rightarrow 2p$ and leads to the reduced pre-edge intensity. Conversely, a many-body perturbation theory, such as the BSE, considers the evolution of many-electron systems using diagrammatic approaches, which is capable of capturing the correct time-ordering and dynamics in photoexcitations. This can be seen in Eq. (3), the BSE begins with empty initial-state orbitals and considers their hybridiza-

tion under the core-hole effect, hence retrieving the edge sharpness.

Many-Electron Formalism To alleviate the deficiencies of the one-body ΔSCF method, we seek a better approximation to $\langle\Psi_f|\boldsymbol{\epsilon}\cdot\boldsymbol{R}|\Psi_i\rangle$ so as to incorporate the many-electron response as the system evolves from the initial to final state. We abandon the single-particle approximation used in Eq. (2) and develop an approximate many-electron wavefunction. To avoid solving an intractable full configuration-interaction problem and leverage the current ΔSCF approach, we assume that the valence Kohn-Sham (KS) orbitals are *non-interacting*. Consequently, a single Slater determinant comprising the KS orbitals is a consistent many-electron eigenstate. This approximation is analogous to the independent-electron model with a single core-hole considered in the MND theory[15, 16]. It may fail to capture certain many-body correlations and we will defer this discussion until later.

Within the independent-KS-orbital approximation, the ground state $|\Psi_i\rangle$ can be constructed as a Slater determinant built from the N lowest occupied valence orbitals of the pristine supercell and the core orbital of the impurity atom. Here, N is the number of valence electrons in the supercell. Similarly, the final state $|\Psi_f\rangle$ can be constructed as a Slater determinant of arbitrary $N+1$ KS orbitals in the final-state picture. To enumerate the many-electron final states, we generalize the final state index f to represent any excited configuration of these $N + 1$ electrons: f now represents a unique $(N + 1)$-tuple, $f = (f_1, f_2, \cdots, f_{N+1})$, where f_i's label distinct final-state orbitals that the $N + 1$ electrons can occupy.

The single-particle orbitals necessary for constructing $|\Psi_i\rangle$ and $|\Psi_f\rangle$ can be readily obtained from respective ΔSCF calculations performed over the supercell. However, $|\Psi_i\rangle$ and $|\Psi_f\rangle$ are represented with the initial- and final-state orbital basis respectively. To eventually access $\langle\Psi_f|\boldsymbol{\epsilon}\cdot\boldsymbol{R}|\Psi_i\rangle$, we perform the orbital transformation from the initial to final state: $|\tilde{\psi}_i\rangle = \sum_j |\psi_j\rangle\langle\psi_j|\tilde{\psi}_i\rangle = \sum_j \xi_{ij}|\psi_j\rangle$, in which $\tilde{\psi}_i$ and ψ_j are the ith final-state and j^{th} initial-state orbitals in the supercell, respectively. ξ_{ij} is the transformation coefficient. The resulting matrix element has the same form as in Eq. (3) but the amplitude of a given final state f becomes a single determinant of the transformation coefficients [56]

$$A_c^f = \det \begin{bmatrix} \xi_{f_1,1} & \xi_{f_1,2} & \cdots & \xi_{f_1,N} & \xi_{f_1,c} \\ \xi_{f_2,1} & \xi_{f_2,2} & \cdots & \xi_{f_2,N} & \xi_{f_2,c} \\ \vdots & & \ddots & & \vdots \\ \xi_{f_{N+1},1} & \xi_{f_{N+1},2} & \cdots & \xi_{f_{N+1},N} & \xi_{f_{N+1},c} \end{bmatrix} \quad (4)$$

Within the independent-KS-orbital approximation, the energy of $|\Psi_f\rangle$ can be found by summing up the en-
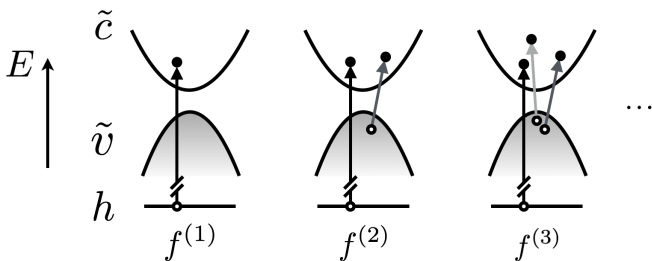
FIG. 3. Schematic of the excitation configurations in the *final-state* space. h indicates the single core level while $\tilde{c}$ and $\tilde{v}$ indicate the empty and occupied orbital spaces respectively.

ergies of the occupied KS orbitals in the *final state*

$$E_f = \sum_{j=1}^{N+1} \tilde{\varepsilon}_{f_j} \qquad (5)$$

The energy difference $E_f - E_i$ for producing spectra may employ a similar alignment scheme as in the single-body approach, since the initial(ground)-state energy E_i is fixed. In the following discussion, it is more meaningful to define the relative energy $\Omega_f = E_f - E_{\mathrm{th}}$, where the threshold energy, $E_{\mathrm{th}} = \sum_{j=1}^{N+1} \tilde{\varepsilon}_j$, corresponds to the lowest-energy final-state configuration $(1, 2, ..., N+1)$.

Determinant expressions similar to Eq. (4) were also obtained in previous work [52–54] but they are rarely applied in a solid-state context from first-principles. Thus it is of great interest to examine whether the many-electron ΔSCF formalism in Eq. (4) and (5) can reproduce the correct lineshapes for the investigated TMOs.

Evaluating the many-electron A_c^f seems formidable at first glance because a solid contains many electrons, which leads to a combinatorially huge number of final states. To facilitate the calculation, we regroup the final-state configurations according to the number of e-h pairs excited. For example, we denote a *single* configuration with one core-excited e-h pair as $f^{(1)} = (1, 2, \cdots, N, f_{N+1})$, which is used in producing the one-body ΔSCF XAS and f_{N+1} is the single unoccupied orbital in the final state. Based on this configuration, we can define a *double* configuration with one more valence e-h pairs as $f^{(2)} = (1, \cdots, i-1, i+1, \cdots, N, f_N, f_{N+1})$, where $f_{N+1} > f_N > N$, and so forth (Fig. 3).

Despite a large number of excitation configurations, not all of them contribute equally to the near-edge XAS, particularly near the absorption onset. First, for an insulator, Ω_f will increase proportionally with the number n of e-h pairs excited across the band gap (E_{g}): $\Omega_f \geq (n-1)E_{\mathrm{g}}$. This significantly reduces the number of necessary final-states for producing the first few eVs of XAS for an insulator. Second, the many-electron transition amplitude may decrease rapidly with increasing number of e-h pairs excited, as we will show next.

We reexamine two extreme cases: the insulating TiO$_2$ and the metallic CrO$_2$. Fig. 4 shows the XAS calcu-
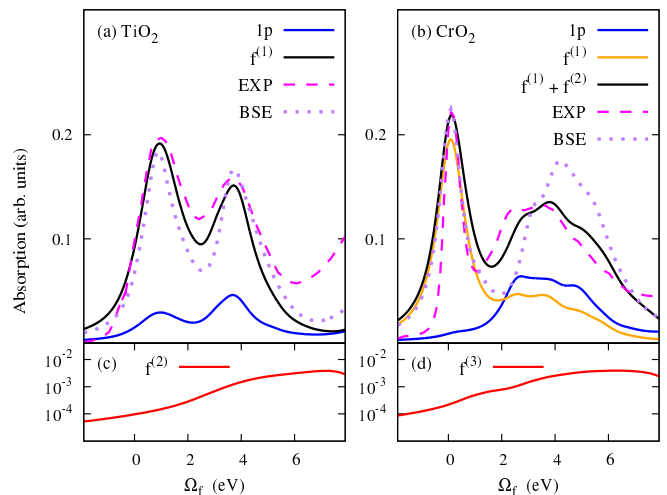

FIG. 4. (Color Online) ΔSCF XAS rectified by the many-electron matrix formalism for TiO$_2$ (a) and CrO$_2$ (b). For comparison, the spectra produced by the one-body FCH formalism are denoted as 1p, and experimental (EXP) and BSE spectra as in Fig. 1 are also added with the first peaks aligned. (c) and (d) show the higher-order intensity contributions (in log scale) that do not exceed 0.004 in both cases.

lated from the many-body formalism as in Eq. (4) and (5). The orbitals used for calculating the transformation coefficients ξ_{ij} in A_c^f are obtained from the same set of ground-state and FCH calculations [56] as previously described. For simplicity, only the states at the Γ-point of the supercell Brillouin zone are used for producing the XAS. Remarkably, the simulated XAS lineshapes (Fig 4) with the many-electron formalism are in excellent agreement with experiments. In particular for CrO$_2$, the edge sharpness is completely retrieved (Fig 4 (b)) despite the disappearance of the first peak in a single-electron theory.

We find calculated XAS for TiO$_2$ converges at the order of $f^{(1)}$. As expected, the contributions from $f^{(2)}$ (Fig 4 (c)) appear at higher energies due to the sizable band gap, and are much weaker due to reduced wavefunction overlap. However, it is more challenging to achieve numerical convergence in the metallic CrO$_2$. While the first peak is retrieved mainly from $f^{(1)}$ excitations, the correct peak-intensity ratio can only be reproduced when the next-order, $f^{(2)}$, is taken into account, which substantially increases the intensity of the absorption feature ~ 4 eV above onset (Fig 4 (b)). Meanwhile, we find $f^{(3)}$ can be neglected up to the first 8 eV (Fig 4 (d)).

Both the BSE (Fig. 1) and the many-electron formalism (Fig 4) yield very similar spectra for TiO$_2$, but the many-electron formalism produces a spectrum for CrO$_2$ in closer agreement with experiment than the BSE. The experimental peak-intensity ratio is 1.7; 1.6 from the many-electron formalism; but only 1.3 from the BSE. We attribute this improvement the explicit inclusion of many-electron response to the core-hole potential via the

transition amplitude A_c^f [Eq. (4)]. Since the Slater determinants are exact solutions to the independent-electron model, the many-electron formalism has taken into account all possible many-electron processes in the MND theory. In addition to the $e\text{-}h$ ladder diagrams in the BSE, the MND theory also considers non-ladder diagrams, such as diagrams with crossing Coulomb lines and bubble diagrams that account for the orthogonality catastrophe [15, 16, 52]. Instead of adopting a diagrammatic approach, the many-electron formalism considers theses processes via incorporating response of each electron to the core hole in the determinant amplitude A_c^f. Therefore, the many-electron formalism goes beyond the two-particle correlation in the BSE. For insulators like TiO$_2$, the many-electron formalism produces results very similar to the BSE because the non-ladder diagrams are not important near the absorption edge. However, this is not the case for CrO$_2$ since multiple $e\text{-}h$-pair production is more likely in a metal and the non-ladder diagrams become significant for determining the near-edge lineshape. The significance of the multiple electron response can also be appreciated from the fact that the CrO$_2$ spectrum converges at a higher-order $f^{(n)}$.

At last, we briefly discuss the validity of the independent-KS-orbital approximation. On the $f^{(1)}$ level, there is a one-to-one correspondence between the many-electron configurations and the empty single-particle final-state orbitals, and the latter are typically good approximations to QP band topology and wavefunctions [43, 55]. This approximation may break down if there are one or more valence $e\text{-}h$ pairs. For example, valence $e\text{-}h$ pairs in the $f^{(2)}$ configurations of an insulator may hybridize to form bound excitons; the two excited electrons in the $f^{(2)}$ configurations may interact through strong on-site Coulomb repulsion. In the case of CrO$_2$, however, the strong metallic screening can largely reduce $e\text{-}h$ binding energy, maintaining the independent-KS-orbital approximation. As for strongly correlated effects, it will be worthwhile to further consider embedded models based on the current determinant formalism.

Conclusions We have shown that the BSE and a newly developed many-electron ΔSCF approach are highly predictive for O K-edge fingerprints of TMOs. The systematic underestimation of the peak-intensity ratio within the original one-body ΔSCF approach is attributed to the absence of many-electron response in this formalism. We have demonstrated how to rectify these shortcomings by (1) extending the wavefunctions in the original ΔSCF to a many-electron form (2) calculating the determinant form of the transition amplitude. This many-electron formalism is transferable and not at all peculiar to TMOs. We leave the discussion of shakeup effects, improvement of efficiency, and other examples to near-future work.

[1] Janel S Uejio, Craig P Schwartz, Richard J Saykally, and David Prendergast. Effects of vibrational motion on core-level spectra of prototype organic molecules. *Chemical Physics Letters*, 467(1):195–199, 2008.

[2] L Triguero, LGM Pettersson, and H Ågren. Calculations of near-edge x-ray-absorption spectra of gas-phase and chemisorbed molecules by means of density-functional and transition-potential theory. *Physical Review B*, 58(12):8097, 1998.

[3] Teruyasu Mizoguchi, Isao Tanaka, Masato Yoshiya, Fumiyasu Oba, Kazuyoshi Ogasawara, and Hirohiko Adachi. Core-hole effects on theoretical electron-energy-loss near-edge structure and near-edge x-ray absorption fine structure of MgO. *Physical Review B*, 61(3):2180, 2000.

[4] Shang-Di Mo and WY Ching. Ab initio calculation of the core-hole effect in the electron energy-loss near-edge structure. *Physical Review B*, 62(12):7901, 2000.

[5] G Duscher, R Buczko, SJ Pennycook, and Sl T Pantelides. Core-hole effects on energy-loss near-edge structure. *Ultramicroscopy*, 86(3):355–362, 2001.

[6] Mathieu Taillefumier, Delphine Cabaret, Anne-Marie Flank, and Francesco Mauri. X-ray absorption near-edge structure calculations with the pseudopotentials: Application to the k edge in diamond and α-quartz. *Physical Review B*, 66(19):195107, 2002.

[7] Balázs Hetényi, Filippo De Angelis, Paolo Giannozzi, and Roberto Car. Calculation of near-edge x-ray-absorption fine structure at finite temperatures: Spectral signatures of hydrogen bond breaking in liquid water. *The Journal of chemical physics*, 120(18):8632–8637, 2004.

[8] Matteo Cavalleri, Michael Odelius, Dennis Nordlund, Anders Nilsson, and Lars GM Pettersson. Half or full core hole in density functional theory x-ray absorption spectrum calculations of water? *Physical Chemistry Chemical Physics*, 7(15):2854–2858, 2005.

[9] David Prendergast and Giulia Galli. X-ray absorption spectra of water from first principles calculations. *Physical Review Letters*, 96(21):215502, 2006.

[10] Juan-Jesus Velasco-Velez, Cheng Hao Wu, Tod A Pascal, Liwen F Wan, Jinghua Guo, David Prendergast, and Miquel Salmeron. The structure of interfacial water on gold electrodes studied by x-ray absorption spectroscopy. *Science*, 346(6211):831–834, 2014.

[11] Eric L Shirley. Ab initio inclusion of electron-hole attraction: Application to x-ray absorption and resonant inelastic x-ray scattering. *Physical Review Letters*, 80(4):794, 1998.

[12] Lorin X Benedict, Eric L Shirley, and Robert B Bohn. Optical absorption of insulators and the electron-hole interaction: An ab initio calculation. *Physical review letters*, 80(20):4514, 1998.

[13] JJ Rehr, JA Soininen, and EL Shirley. Final-state rule vs the bethe-salpeter equation for deep-core x-ray absorption spectra. *Physica Scripta*, 2005(T115):207, 2005.

[14] J Vinson, JJ Rehr, JJ Kas, and EL Shirley. Bethe-salpeter equation calculations of core excitation spectra. *Physical Review B*, 83(11):115106, 2011.

[15] Ph Nozieres and CT De Dominicis. Singularities in the x-ray absorption and emission of metals. iii. one-body theory exact solution. *Physical Review*, 178(3):1097, 1969.

[16] Gerald D Mahan. *Many-particle physics*. Springer Science & Business Media, 2013.

[17] Naoaki Yabuuchi, Kazuhiro Yoshii, Seung-Taek Myung, Izumi Nakai, and Shinichi Komaba. Detailed studies of a high-capacity electrode material for rechargeable batteries Li_2MnO_3-$LiCo_{1/3}Ni_{1/3}Mn_{1/3}O_2$ *Journal of the American Chemical Society*, 133(12):4404–4419, 2011.

[18] Yan-Yan Hu, Zigeng Liu, Kyung-Wan Nam, Olaf J Borkiewicz, Jun Cheng, Xiao Hua, Matthew T Dunstan, Xiqian Yu, Kamila M Wiaderek, Lin-Shu Du, et al. Origin of additional capacities in metal oxide lithium-ion battery electrodes. *Nature materials*, 12(12):1130–1136, 2013.

[19] Feng Lin, Dennis Nordlund, Yuyi Li, Matthew K Quan, Lei Cheng, Tsu-Chien Weng, Yijin Liu, Huolin L Xin, and Marca M Doeff. Metal segregation in hierarchically structured cathode materials for high-energy lithium batteries. *Nature Energy*, 1:15004, 2016.

[20] Kun Luo, Matthew R Roberts, Rong Hao, Niccoló Guerrini, David M Pickup, Yi-Sheng Liu, Kristina Edström, Jinghua Guo, Alan V Chadwick, Laurent C Duda, et al. Charge-compensation in 3d-transition-metal-oxide intercalation cathodes through the generation of localized electron holes on oxygen. *Nature Chemistry*, 2016.

[21] Jin Suntivich, Hubert A Gasteiger, Naoaki Yabuuchi, Haruyuki Nakanishi, John B Goodenough, and Yang Shao-Horn. Design principles for oxygen-reduction activity on perovskite oxide catalysts for fuel cells and metal–air batteries. *Nature chemistry*, 3(7):546–550, 2011.

[22] Peter Strasser, Shirlaine Koh, Toyli Anniyev, Jeff Greeley, Karren More, Chengfei Yu, Zengcai Liu, Sarp Kaya, Dennis Nordlund, Hirohito Ogasawara, et al. Lattice-strain control of the activity in dealloyed core–shell fuel cell catalysts. *Nature chemistry*, 2(6):454–460, 2010.

[23] Guo-zhen Zhu, Guillaume Radtke, and Gianluigi A Botton. Bonding and structure of a reconstructed (001) surface of srtio3 from tem. *Nature*, 490(7420):384–387, 2012.

[24] Michinori Matsukawa, Ryo Ishikawa, Takashi Hisatomi, Yosuke Moriya, Naoya Shibata, Jun Kubota, Yuichi Ikuhara, and Kazunari Domen. Enhancing photocatalytic activity of latio2n by removal of surface reconstruction layer. *Nano letters*, 14(2):1038–1041, 2014.

[25] Alexis Grimaud, Kevin J May, Christopher E Carlton, Yueh-Lin Lee, Marcel Risch, Wesley T Hong, Jigang Zhou, and Yang Shao-Horn. Double perovskites as a family of highly active catalysts for oxygen evolution in alkaline solution. *Nature communications*, 4, 2013.

[26] Z Lebens-Higgins, DO Scanlon, H Paik, S Sallis, Y Nie, M Uchida, NF Quackenbush, MJ Wahila, GE Sterbinsky, Dario A Arena, et al. Direct observation of electrostatically driven band gap renormalization in a degenerate perovskite transparent conducting oxide. *Phys Rev Lett*, 116:027602, 2016.

[27] TC Koethe, Z Hu, MW Haverkort, C Schüßler-Langeheine, F Venturini, NB Brookes, Oscar Tjernberg, W Reichelt, HH Hsieh, H-J Lin, et al. Transfer of spectral weight and symmetry across the metal-insulator transition in vo 2. *Physical review letters*, 97(11):116402, 2006.

[28] Dmitry Ruzmetov, Sanjaya D Senanayake, and Shriram Ramanathan. X-ray absorption spectroscopy of vanadium dioxide thin films across the phase-transition boundary. *Physical Review B*, 75(19):195102, 2007.

[29] Nagaphani B Aetukuri, Alexander X Gray, Marc Drouard, Matteo Cossale, Li Gao, Alexander H Reid, Roopali Kukreja, Hendrik Ohldag, Catherine A Jenkins, Elke Arenholz, et al. Control of the metal-insulator transition in vanadium dioxide by modifying orbital occupancy. *Nature Physics*, 9(10):661–666, 2013.

[30] CT Chen, F Sette, Y Ma, MS Hybertsen, EB Stechel, WMC Foulkes, M Schulter, SW Cheong, AS Cooper, LW Rupp Jr, et al. Electronic states in la 2- x sr x cuo 4+ δ probed by soft-x-ray absorption. *Physical review letters*, 66(1):104, 1991.

[31] DC Peets, DG Hawthorn, KM Shen, Young-June Kim, DS Ellis, H Zhang, Seiki Komiya, Yoichi Ando, GA Sawatzky, Ruixing Liang, et al. X-ray absorption spectra reveal the inapplicability of the single-band hubbard model to overdoped cuprate superconductors. *Physical review letters*, 103(8):087402, 2009.

[32] J-S Lee, YW Xie, HK Sato, C Bell, Y Hikita, HY Hwang, and C-C Kao. Titanium dxy ferromagnetism at the laalo3/srtio3 interface. *Nature materials*, 12(8):703–706, 2013.

[33] SL Dudarev, GA Botton, SY Savrasov, CJ Humphreys, and AP Sutton. Electron-energy-loss spectra and the structural stability of nickel oxide: An lsda+ u study. *Physical Review B*, 57(3):1505, 1998.

[34] VI Anisimov, Dm M Korotin, MA Korotin, AV Kozhevnikov, J Kuneš, AO Shorikov, SL Skornyakov, and SV Streltsov. Coulomb repulsion and correlation strength in lafeaso from density functional and dynamical mean-field theories. *Journal of Physics: Condensed Matter*, 21(7):075602, 2009.

[35] Xin Wang, Luca de?Medici, and AJ Millis. Theory of oxygen k edge x-ray absorption spectra of cuprates. *Physical Review B*, 81(9):094522, 2010.

[36] C-C Chen, M Sentef, YF Kung, CJ Jia, R Thomale, B Moritz, AP Kampf, and TP Devereaux. Doping evolution of the oxygen k-edge x-ray absorption spectra of cuprate superconductors using a three-orbital hubbard model. *Physical Review B*, 87(16):165144, 2013.

[37] Wensheng Yan, Zhihu Sun, Zhiyun Pan, Qinghua Liu, Tao Yao, Ziyu Wu, Cheng Song, Fei Zeng, Yaning Xie, Tiandou Hu, et al. Oxygen vacancy effect on room-temperature ferromagnetism of rutile co: Tio2 thin films. *Applied Physics Letters*, 94(4):42508, 2009.

[38] CB Stagarescu, X Su, DE Eastman, KN Altmann, FJ Himpsel, and A Gupta. Orbital character of o- 2 p unoccupied states near the fermi level in cro 2. *Physical Review B*, 61(14):R9233, 2000.

[39] Shaohua Shen, Jigang Zhou, Chung-Li Dong, Yongfeng Hu, Eric Nestor Tseng, Penghui Guo, Liejin Guo, and Samuel S Mao. Surface engineered doping of hematite nanorod arrays for improved photoelectrochemical water splitting. *Scientific reports*, 4, 2014.

[40] JJ Rehr, J Mustre de Leon, SI Zabinsky, and RC Albers. Theoretical x-ray absorption fine structure standards. *Journal of the American chemical society*, 113(14):5135–5140, 1991.

[41] Peng Jiang, David Prendergast, Ferenc Borondics, Soeren Porsgaard, Lisandro Giovanetti, Elzbieta Pach, John Newberg, Hendrik Bluhm, Flemming Besenbacher, and Miquel Salmeron. Experimental and theoretical investigation of the electronic structure of cu2o and cuo thin films on cu (110) using x-ray photoelectron and absorption spectroscopy. *The Journal of chemical physics*, 138(2):024704, 2013.

[42] Lei Wang, Thomas Maxisch, and Gerbrand Ceder. Oxidation energies of transition metal oxides within the gga+ u framework. *Physical Review B*, 73(19):195107, 2006.

[43] Michael Rohlfing and Steven G Louie. Electron-hole excitations and optical spectra from first principles. *Physical Review B*, 62(8):4927, 2000.

[44] Giovanni Onida, Lucia Reining, and Angel Rubio. Electronic excitations: density-functional versus many-body green?s-function approaches. *Reviews of Modern Physics*, 74(2):601, 2002.

[45] K Gilmore, John Vinson, EL Shirley, D Prendergast, CD Pemmaraju, JJ Kas, FD Vila, and JJ Rehr. Efficient implementation of core-excitation bethe–salpeter equation calculations. *Computer Physics Communications*, 197:109–117, 2015.

[46] Frank De Groot and Akio Kotani. *Core level spectroscopy of solids*. CRC press, 2008.

[47] Frank De Groot. High-resolution x-ray emission and x-ray absorption spectroscopy. *Chemical Reviews*, 101(6):1779–1808, 2001.

[48] FMF De Groot, M Grioni, JC Fuggle, J Ghijsen, GA Sawatzky, and H Petersen. Oxygen 1s x-ray-absorption edges of transition-metal oxides. *Physical Review B*, 40(8):5715, 1989.

[49] Amélie Juhin, Frank De Groot, György Vankó, Matteo Calandra, and Christian Brouder. Angular dependence of core hole screening in licoo 2: A dft+ u calculation of the oxygen and cobalt k-edge x-ray absorption spectra. *Physical Review B*, 81(11):115115, 2010.

[50] Isao Tanaka, Teruyasu Mizoguchi, and Tomoyuki Yamamoto. Xanes and elnes in ceramic science. *Journal of the American Ceramic Society*, 88(8):2013–2029, 2005.

[51] V Kanchana, G Vaitheeswaran, and M Alouani. Calculated electronic structure and x-ray magnetic circular dichroism of cro2. *Journal of Physics: Condensed Matter*, 18(22):5155, 2006.

[52] PHILIP W Anderson. Infrared catastrophe in fermi gases with local scattering potentials. *Physical Review Letters*, 18(24):1049, 1967.

[53] Edward A Stern and John J Rehr. Many-body aspects of the near-edge structure in x-ray absorption. *Physical Review B*, 27(6):3351, 1983.

[54] K Ohtaka and Y Tanabe. Theory of the soft-x-ray edge problem in simple metals: historical survey and recent developments. *Reviews of Modern Physics*, 62(4):929, 1990.

[55] Mark S Hybertsen and Steven G Louie. Electron correlation in semiconductors and insulators: Band gaps and quasiparticle energies. *Physical Review B*, 34(8):5390, 1986.

[56] See Supplemental Material [url], which includes Refs. [57-58].

[57] Paolo Giannozzi, Stefano Baroni, Nicola Bonini, Matteo Calandra, Roberto Car, Carlo Cavazzoni, Davide Ceresoli, Guido L Chiarotti, Matteo Cococcioni, Ismaila Dabo, Andrea Dal Corso, Stefano de Gironcoli, Stefano Fabris, Guido Fratesi, Ralph Gebauer, Uwe Gerstmann, Christos Gougoussis, Anton Kokalj, Michele Lazzeri, Layla Martin-Samos, Nicola Marzari, Francesco Mauri, Riccardo Mazzarello, Stefano Paolini, Alfredo Pasquarello, Lorenzo Paulatto, Carlo Sbraccia, Sandro Scandolo, Gabriele Sclauzero, Ari P Seitsonen, Alexander Smogunov, Paolo Umari, and Renata M Wentzcovitch. Quantum espresso: a modular and open-source software project for quantum simulations of materials. *Journal of Physics: Condensed Matter*, 21(39):395502 (19pp), 2009.

[58] Eric L Shirley. Optimal basis sets for detailed brillouin-zone integrations. *Physical Review B*, 54(23):16464, 1996.